

- 4981 Chemical weathering shapes continents  
 5099 Single amyloid  $\beta$ -peptide examined  
 5105 Faster path to drug cocktails  
 5166 MicroRNA's influence on leukemia  
 5172 Designer T cells prevent autoimmune disease in mice

## GEOLOGY, EVOLUTION

**Chemical weathering shapes continents**

Continental crust rises higher than oceanic crust because it is less dense: It is rich in Si and poor in Mg. However, basalt, which is derived from magma, is denser and has a higher ratio of Mg to Si than the rock that makes up mature continental crust. Cin-Ty Lee *et al.* argue that chemical weathering alters the composition of continental crust as it ages and helps give it its more buoyant character. Both chemical weathering and “delamination” of Mg-rich lower crust, which occurs as it peels off and reenters the mantle, have been proposed as mechanisms that remove Mg from continents. However, quantifying the relative strength of chemical weathering versus delamination has long been a challenge. The problem is essentially that two equations arise to explain the removal of Mg, but the equations contain three unknowns and therefore cannot be solved. The authors observe that the weathering of Li and Mg is coupled, which allows the system to be solved. The authors report that chemical weathering accounts for a loss of 20% of the original basalt Mg compared with a 40% loss by other routes. From this perspective, it seems possible that life, by altering crustal chemistry via weathering, can affect the evolution of continents. — K.M.

“Regulating continent growth and composition by chemical weathering” by Cin-Ty Aeolus Lee, Douglas M. Morton, Mark G. Little, Ronald Kistler, Ulyana N. Horodyskyj, William P. Leeman, and Arnaud Agranier (see pages 4981–4986)

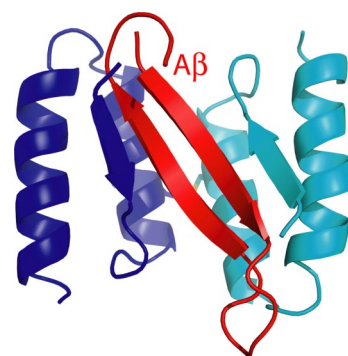
## BIOPHYSICS

**Single amyloid  $\beta$ -peptide examined**

The aggregation of misfolded amyloid  $\beta$ -peptide protein into plaques is thought to be a primary cause of Alzheimer's disease. Wolfgang Hoyer *et al.* report on the detailed structure of the  $\beta$ -hairpin in a single misfolded Alzheimer's amyloid  $\beta$ -peptide. The authors bound the 40-aa isoform of the amyloid  $\beta$ -peptide to an engineered affinity protein and examined it with nuclear magnetic resonance spectroscopy. They found that amino acids 17–36 form the  $\beta$ -hairpin. The isolated hairpin

strongly resembled fibrillar amyloid  $\beta$ -peptide. The authors found that the affinity protein stabilizes the  $\beta$ -sheet by extending it intermolecularly and by burying both of the mostly nonpolar faces of the amyloid  $\beta$ -hairpin within a large hydrophobic tunnel-like cavity. They show that the affinity protein inhibits the formation of fibrillar amyloid  $\beta$ -peptide. This conformation is a step toward identifying the oligomerization and fibrillation that leads to Alzheimer's disease, according to the authors. — P.D.

“Stabilization of a  $\beta$ -hairpin in monomeric Alzheimer's amyloid- $\beta$  peptide inhibits amyloid formation” by Wolfgang Hoyer, Caroline Grönwall, Andreas Jonsson, Stefan Ståhl, and Torleif Hård (see pages 5099–5104)

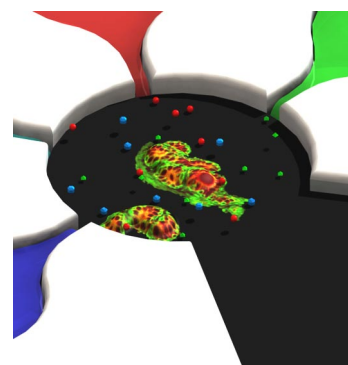


The  $\beta$ -hairpin of amyloid- $\beta$  peptide (red), bound to an affinity protein.

## CELL BIOLOGY, ENGINEERING

**Faster path to drug cocktails**

A finely tuned drug cocktail is often more effective than a single drug. Finding the appropriate drug combinations in the vast realm of possibilities is much faster using a feedback control technique developed by Pak Kin Wong *et al.* In addition to the challenge posed by testing all possible drug combinations at varying doses is the need to consider their action in a biological system. To optimize combinations without requiring detailed information about individual biological pathways and interactions, the authors developed an experimental closed-loop control scheme



Closed-loop feedback control scheme.

integrated with a search algorithm to identify the cocktail based on the response of the biological system as a whole. The algorithm develops its next iteration only after feedback, in this case a series of discernible phenotypic responses. The authors used the closed-loop control scheme to reduce infection of cultured cells with a mammalian virus. This approach rapidly identified a combination of drugs that inhibited almost 100% of viral activity, with lower doses of each than would be needed alone. — T.H.D.

“Closed-loop control of cellular functions using combinatory drugs guided by a stochastic search algorithm” by Pak Kin Wong, Fuqu Yu, Arash Shahangian, Genhong Cheng, Ren Sun, and Chih-Ming Ho (see pages 5105–5110)

## GENETICS

### MicroRNA's influence on leukemia

MicroRNAs have been predicted to influence diseases by regulating hundreds of gene transcripts at a time, but few such data sets have been identified. George Calin *et al.* present evidence that miR-15a and miR-16-1, which are known to suppress tumors through the BCL2 oncogene, activate and inactivate many genes that are implicated in human leukemia. The authors inserted the miRNAs into the genomes of tumor cells and injected them into nude mice.



Comparison of tumor growth in nude mice.

The miRNA clusters completely suppressed tumor growth in three of five mice and shrunk the tumors in other mice. The miRNAs also

up-regulated 265 genes and down-regulated 3,307, meaning that  $\approx 14\%$  of the estimated number of human genes were affected. Among the many genes that were down-regulated, a significant number had AU-rich elements. An analysis of the down-regulated transcripts identified many genes that are activated in cancer by directly or indirectly affecting apoptosis and the cell cycle. The authors say that identifying the suite of silenced genes could help develop new therapies for leukemia. — P.D.

“MiR-15a and miR-16-1 cluster functions in human leukemia” by George A. Calin, Amelia Cimmino, Muller Fabbri, Manuela Ferracin, Sylwia E. Wojcik, Masayoshi Shimizu, Cristian Taccioli, Nicola Zanasi, Ramiro Garzon, Rami I. Aqeilan, Hansjuerg Alder, Stefano Volinia, Laura Rassenti, Xiuping Liu, Chang-gong Liu, Thomas J. Kipps, Massimo Negrini, and Carlo M. Croce (see pages 5166–5171)

## IMMUNOLOGY

### Designer T cells prevent autoimmune disease in mice

Multiple sclerosis (MS) is an autoimmune disease that occurs when the body's T cells attack the fatty myelin sheath that insulates nerve fibers in the brain, spinal cord, and optic nerve. Without this protective layer, nerves are unable to send electrical signals and scars are formed. Joel Stern *et al.* developed regulatory T cell lines that suppress multiple autoimmune diseases in mice, including experimental autoimmune encephalomyelitis (EAE), the mouse model of MS. To create these MS-fighting T cells, Stern *et al.* immunized SJL/J mice with amino acid copolymers, then harvested T lymphocytes from the spleen and lymph nodes and used the lymphocytes to create cell lines. These new T cell lines secrete high levels of IL-10 and IL-13-immune chemicals that play an important role in immunosuppression. However, unlike traditional T cells, these lines only produce small amounts of IL-4 and virtually no TGF- $\beta$ , IL-17, IL-6, IL-2, IFN- $\gamma$ , or TNF $\alpha$ . When EAE was triggered in genetically susceptible mice, the animals developed disease at day 17 or 18. However, animals that received the IL-10-secreting T cells failed to develop EAE. The T cells also prevented the development of two other autoimmune diseases that could be induced in the same strain of mice. — B.T.

“Amino acid copolymer-specific IL-10-secreting regulatory T cells that ameliorate autoimmune diseases in mice” by Joel N. H. Stern, Derin B. Keskin, Hong Zhang, HuiJuan Lv, Zenichiro Kato, and Jack L. Strominger (see pages 5172–5176)

# Closed-loop control of cellular functions using combinatory drugs guided by a stochastic search algorithm

Pak Kin Wong\*<sup>†</sup>, Fuqu Yu<sup>‡</sup>, Arash Shahangian<sup>§</sup>, Genhong Cheng<sup>§¶</sup>, Ren Sun<sup>‡</sup>, and Chih-Ming Ho<sup>\*¶||</sup>

\*Department of Aerospace and Mechanical Engineering and Bio5 Institute, University of Arizona, N718, 1130 North Mountain Avenue, Tucson, AZ 85721; <sup>†</sup>Department of Molecular and Medical Pharmacology, University of California, 10-240 Factor, 420 Westwood Plaza, Los Angeles, CA 90095; <sup>‡</sup>Department of Microbiology, Immunology and Molecular Genetics, University of California, 8-240 J, Factor Building, 10833 Le Conte Avenue, Los Angeles, CA 90095; <sup>§</sup>Department of Mechanical and Aerospace Engineering, University of California, Eng IV 38-137 J, 420 Westwood Plaza, Los Angeles, CA 90095; and <sup>¶</sup>Center for Cell Control, University of California, Los Angeles, CA 90095

Communicated by Leroy L. Chang, Hong Kong University of Science and Technology, Clear Water Bay, Hong Kong SAR, January 26, 2008 (received for review July 8, 2007)

**A mixture of drugs is often more effective than using a single effector. However, it is extremely challenging to identify potent drug combinations by trial and error because of the large number of possible combinations and the inherent complexity of the underlying biological network. With a closed-loop optimization modality, we experimentally demonstrate effective searching for potent drug combinations for controlling cellular functions through a large parametric space. Only tens of iterations out of one hundred thousand possible trials were needed to determine a potent combination of drugs for inhibiting vesicular stomatitis virus infection of NIH 3T3 fibroblasts. In addition, the drug combination reduced the required dosage by  $\approx 10$ -fold compared with individual drugs. In another example, a potent mixture was identified in thirty iterations out of a possible million combinations of six cytokines that regulate the activity of nuclear factor kappa B in 293T cells. The closed-loop optimization approach possesses the potential of being an effective approach for manipulating a wide class of biological systems.**

combinatory drug therapy | drug cocktail | drug resistance | feedback control | viral infection

Diseases arise from altered cellular functions and activities. Modifying cellular activities by a combination of agonists can lead to an effective strategy for disease therapeutics. A mixture of drugs, in many cases, is more effective than using a single stimulus (1–5). However, the combination of various possible concentrations of a set of agonists creates a large testing parametric space. As such, identifying the optimum combination of multiple drugs to control a complex biological system presents a major challenge (6, 7). Here, we experimentally demonstrate that a closed-loop optimization scheme can serve as an alternative approach to trial and error, which needs to test a large number of all of the possible combinations. The approach suggested in this work effectively searches for potent drug combinations that manipulate the cellular network toward a therapeutic goal.

Cellular functions and activities are regulated by complex networks of signaling and regulatory pathways. The current approach aims to circumvent the need for detailed information of biological signaling and regulatory networks. To experimentally implement the closed-loop optimization approach for searching for a potent drug mixture, combinations of cytokines and drugs are applied to stimulate the system of interest. Biomarkers indicating the biological responses of interest, such as viral activity, are then evaluated. Based on the biological responses, a stochastic search algorithm chooses a new drug mixture for the next test. Iteratively, the closed-loop control scheme will drive the systems to desired phenotypic responses (Fig. 1). We have demonstrated that only tens of iterations out of a large number of possible combinations are needed. This

effort-saving approach actively manipulates the complex biological systems as a whole, rather than analyzing the processes through individual signaling pathways in a network.

The closed-loop control can serve as a generic approach in devising multidrug therapies against wide classes of pathogens and diseases. We have chosen two model systems to explore this closed-loop optimization approach. In the first system, we consider combinations of interferons (IFNs) and antiviral drugs for inhibiting viral activity. Specifically, vesicular stomatitis virus (VSV) infection of NIH 3T3 fibroblasts was used as the model system. Although a combination of cytokines and drugs is known to have a stronger antiviral activity than that from a single agent, the complex interactions among the pathways and the large parametric space constituted by the combinatorial drugs impose a major challenge to identifying potent combinations. In the second system, the activity of nuclear factor kappa B (NF- $\kappa$ B) was chosen as the endpoint. The therapeutic effect of combinatorial cytokines on human embryonic kidney 293T cells was explored by searching for a potent combination of cytokines for maximizing the activity of NF- $\kappa$ B. NF- $\kappa$ B regulates expression of several genes that mediate the inflammatory responses and cell proliferation, and is one of the major therapeutic targets for chronic inflammatory disease and cancer (8, 9).

## Results

**Stochastic Search Algorithm.** Stochastic search algorithms constitute one of the most effective approaches to solving large-scale combinatorial optimization problems of highly complex systems. Stochastic search algorithms do not require training of data to form a metamodel as in surrogate-based optimization (e.g., neural networks) (10). Therefore, only a small number of experiments is typically required. Simulated annealing (11), genetic algorithms (12), ant colony optimization (13), and Gur Game (14) are some of the well established stochastic search algorithms. These algorithms have been demonstrated in a variety of applications, such as crystal structure predications (11), routing in communication networks (13), and distributed control in robotics (16, 17). These methods have also been applied in computational biology (18) and protein-folding stud-

Author contributions: P.K.W., F.Y., G.C., R.S., and C.-M.H. designed research; P.K.W., F.Y., and A.S. performed research; P.K.W., F.Y., A.S., G.C., R.S., and C.-M.H. contributed new reagents/analytic tools; P.K.W., F.Y., A.S., G.C., R.S., and C.-M.H. analyzed data; and P.K.W., F.Y., R.S., and C.-M.H. wrote the paper.

The authors declare no conflict of interest.

Freely available online through the PNAS open access option.

<sup>†</sup>To whom correspondence may be addressed. E-mail: pak@email.arizona.edu or chihming@ucla.edu.

This article contains supporting information online at [www.pnas.org/cgi/content/full/0800823105/DC1](http://www.pnas.org/cgi/content/full/0800823105/DC1).

© 2008 by The National Academy of Sciences of the USA



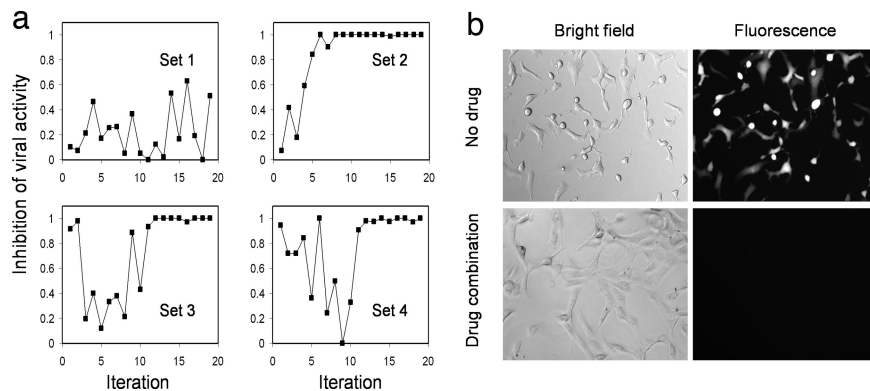


**Fig. 3.** Optimizing antiviral drug combinations with the Gur Game. Inhibition of viral activity is defined as the percentage of uninfected cells (indicated by GFP expression). (a) Four sets of experiments were performed to determine potent drug cocktails. Set 2 converges in <10 iterations and identifies a potent combination that inhibits the viral activity completely. Set 3 and set 4 converge at the 12th and 14th iteration, respectively. (b) Bright field and fluorescence micrographs of NIH 3T3 cells treated with VSV at 1 multiplicity of infection (moi) with and without the drug combination identified in set 2.

reached a potent combination that totally inhibited the GFP expression and converged to the solution in less than ten iterations (Fig. 3). This is likely because of the smaller set of concentrations applied in set 2. Similarly, set 3 and set 4 converged to potent combinations that inhibited 100% of viral activity after 12 and 14 iterations, respectively. The results of set 3 are listed in Table 1 to illustrate a typical iteration of the search process. However, set 1 containing only three types of IFN reached a maximum viral inhibition value of  $\approx 0.63$ , that is, 63% of the cells were not expressing GFP.

**Cytokine Combinations for Activating NF- $\kappa$ B.** To illustrate that the closed-loop control scheme can be applied in different biological systems, we searched for cytokine combinations that regulate NF- $\kappa$ B activity in 293T cells. Six cytokines (TNF $\alpha$ , TNF $\beta$ , IL-1 $\alpha$ , IL-1 $\beta$ , EGF, and BAFF) were considered for regulating the NF- $\kappa$ B activity. The six stimuli, belonging to three families of cytokines and growth factors, represent various possibilities of pathway interactions: (i) effectors trigger different receptors and mechanisms of a single-pathway component, and/or (ii) parallel pathways are triggered simultaneously, each of which exerts effects on a subsequent phenotype. Tumor necrosis factor (TNF) and interleukin 1 (IL-1) are commonly used for stimulating the

NF- $\kappa$ B signal transduction pathway (21). Although TNF $\alpha$ , TNF $\beta$ , IL-1 $\alpha$ , and IL-1 $\beta$  have similar functions, they are known to have distinct roles in the cellular responses (22). Stimulation with TNF $\alpha$  and IL-1 $\beta$  simultaneously was reported to activate NF- $\kappa$ B (23) and other cellular functions (24) synergistically. The effect of epidermal growth factor (EGF) on NF- $\kappa$ B signaling is cell-type specific. For example, EGF has been reported to up-regulate NF- $\kappa$ B activity in several cell lines that have high levels of EGF receptor expression (25). However, EGF does not enhance NF- $\kappa$ B activity in human microvascular endothelial cells (26) and suppresses oxidant-induced NF- $\kappa$ B activity in intestinal epithelial cells (27). BAFF (B cell-activating factor belonging to the TNF family) has been shown to activate NF- $\kappa$ B by a NF- $\kappa$ B essential modulator (NEMO) (IKK $\gamma$ ) independent pathway in maturing B cells (28). The possible interactions of the six cytokines and the resulting combinatorial effects on NF- $\kappa$ B in 293T cell are not fully understood. In this study, each agonist was assigned 10 discrete concentrations: 0, 0.25, 0.5, 1, 2.5, 5, 10, 25, 50, or 100 ng/ml. The values spanned over three orders of magnitude in concentration. The concentrations were selected to maximize the range to be considered while maintaining acceptable resolution in cytokine concentrations (i.e., the difference between concentrations). The lowest concentration that

**Table 1.** List of drug concentrations and random numbers generated by Gur game in viral inhibition experiment of set 3 test

Iteration	IFN $\alpha$ , pg/ml	Random no. IFN $\alpha$	IFN $\beta$ , ng/ml	Random no. IFN $\beta$	IFN $\gamma$ , ng/ml	Random no. IFN $\gamma$	Puromycin, $\mu$ g/ml	Random no. Puromycin	Ribavirin, $\mu$ g/ml	Random no. Ribavirin	Reward
1	7.8	1	0.6	0.23	60	0.2	1.5	0.68	6	0.28	0.92
2	15.6	0.06	0.3	0.5	30	0.14	0.75	0.81	3	0.14	0.98
3	32.5	0.27	0.1	0.72	10	0.26	0.25	0.13	1	0.66	0.2
4	15.6	0.53	0.3	0.7	30	0.84	0.125	0.29	3	0.33	0.4
5	7.8	0.15	0.6	0.86	60	0.65	0	0.51	1	0.13	0.12
6	15.6	0.96	1.2	0.72	120	0.26	0.125	0.46	3	0.25	0.33
7	7.8	0.26	0.6	0.39	250	0.55	0.25	0.88	1	0	0.38
8	3.9	0.93	1.2	0.25	120	0.71	0.75	0.28	0.5	0.59	0.21
9	7.8	0.04	0.6	0.11	60	0.36	1.5	0.9	1	0.99	0.89
10	3.9	0.47	0.3	0.32	30	0.55	3	0.15	3	0.52	0.43
11	7.8	0.6	0.1	0.55	60	0.57	6.25	0.65	6	0.95	0.93
12	3.9	0.35	0.05	0.45	30	0.77	12.5	0.35	12	0.59	1
13	1.3	0.2	0	0.71	10	0.24	25	0.4	25	0.56	1
14	0.65	0.79	0	0.62	5	0.24	50	0.16	50	0.61	1
15	0	0.53	0	0.46	0	0.06	50	0.28	100	0.69	1
16	0	0.76	0	0.2	0	0.45	50	0.51	200	0.03	0.97
17	0	0.19	0	0.24	0	0.03	50	0.73	200	0.4	1
18	0	0.89	0	0.21	0	0.39	50	0.43	200	0.19	1
19	0	0.32	0	0.36	0	0.36	50	0.48	200	0.49	1
20	0		0		0		50		200		

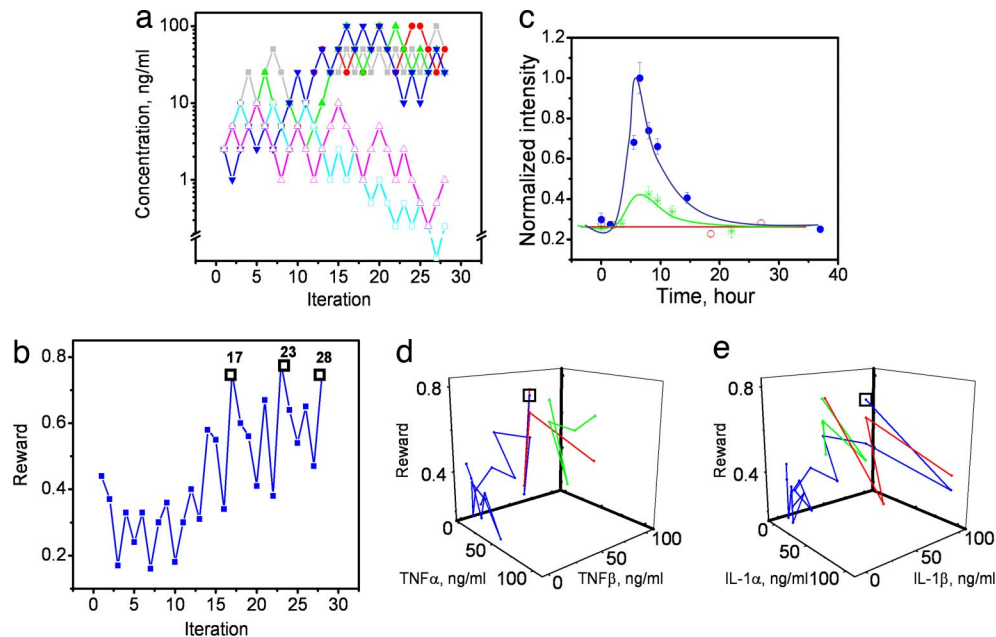


**Fig. 4.** Searching for a cytokine mixture that optimizes NF- $\kappa$ B activity. (a) Concentration of individual cytokines TNF $\alpha$  (gray filled square), TNF $\beta$  (red filled circle), IL-1 $\alpha$  (green filled triangle), IL-1 $\beta$  (blue inverted triangle), EGF (cyan open square), and BAFF (magenta open triangle) applied at different iterations. The initial concentration of all of the cytokines was 2.5 ng/ml. (b) Normalized GFP intensity at different iterations. Iterations 17, 23, and 28 are labeled with black open squares. (c) Dynamic response of NF- $\kappa$ B activity for cells treated with the cytokine combination (blue filled circle), TNF $\alpha$  50 ng/ml (green asterisk), and control (red open circle). Data are normalized to the maximum intensity for cells treated with the cytokine combination. Data represent the mean  $\pm$  SEM from at least 100 cells inside the microfluidic channels. (d) Searching paths for TNF $\alpha$  and TNF $\beta$  and (e) searching paths for IL-1 $\alpha$  and IL-1 $\beta$ . Black open squares represent cytokine concentrations at iteration 17. Each color represents a particular path.

showed an observable effect was between 0.25 and 1 ng/ml. Concentrations  $>100$  ng/ml resulted in a considerable amount of cytotoxicity and, therefore, were not considered in this study. Ten concentrations each of six cytokines led to one million ( $10^6$ ) possible combinations in the search space.

**Closed-Loop Optimization of NF- $\kappa$ B Activity.** The closed-loop optimization experiment started with choosing a set of cytokine concentrations. Then, the cells cultured inside a microfluidic channel were transiently stimulated with the set of cytokines for one hour. The duration is based on previous reports of the dynamic of NF- $\kappa$ B and selected so that no oscillatory response of the NF- $\kappa$ B will take place (29). The fluorescent light is linearly proportional to the NF- $\kappa$ B expression level (30). The GFP fluorescence intensities of individual cells were recorded seven hours after the stimulation at the peak time point of the fluorescence induction. The average GFP intensity of  $\approx 100$  cells was fed to the Gur Game. According to the intensity, the Gur Game determined the concentration of each cytokine for the next iteration. These processes were repeated during each iteration. At the beginning of the experiment, the cytokine concentrations were chosen randomly by the Gur Game to explore cytokine combinations with high NF- $\kappa$ B outputs (Fig. 4 a and b). The system was not trapped by several cytokine combinations with apparently high outputs, e.g., iteration 14. Near iteration 12, the algorithm “detected” a promising trend. Four cytokines (TNF $\alpha$ , TNF $\beta$ , IL-1 $\alpha$ , and IL-1 $\beta$ ) were driven to higher concentrations but the other two (EGF and BAFF) were driven to lower concentrations. At iteration 17, the system determined a potent combination of cytokines for activating the NF- $\kappa$ B. Because of the random walk nature of the Gur Game, the algorithm did not settle with the large performance gains at iteration 17. The most potent cytokine combination was (TNF $\alpha$  = 25 ng/ml, TNF $\beta$  = 50 ng/ml, IL-1 $\alpha$  = 50 ng/ml, IL-1 $\beta$  = 50 ng/ml, EGF = 2.5 ng/ml, BAFF = 2.5 ng/ml). The random walk nature of the algorithm continually looked for other states with better performance, and the

reward function decreased significantly several times during the search. However, the system returned to the similar NF- $\kappa$ B activity at iterations 23 and 28. A comparison between NF- $\kappa$ B activities under stimulation of TNF $\alpha$  and the cytokine combination is shown in Fig. 4c. The searching paths are shown in Fig. 4 d and e.

## Discussion

In the viral infection experiment, we have shown that potent drug combinations can be identified rapidly by using a closed-loop optimization approach. With only tens of experiments, potent drug combinations, which can inhibit close to 100% of VSV activity in NIH 3T3 cells, have been identified. The closed-loop optimization scheme not only enhances the antiviral activity of cytokines and drugs, but also minimizes their dosages. To elucidate the effectiveness of drug cocktails, we compared the antiviral activity of a potent drug mixture (IFN $\alpha$  = 3.9 pg/ml; IFN $\beta$  = 0.05 ng/ml; IFN $\gamma$  = 30 ng/ml; puromycin = 12.5  $\mu$ g/ml; ribavirin = 12  $\mu$ g/ml) with individual drugs. If a single drug is applied, much higher concentrations are required. Fig. 5a shows the dosages required for completely inhibiting the viral activity by using the potent drug combination. If applied individually, concentrations of 100  $\mu$ g/ml and 25  $\mu$ g/ml (Fig. 5b) were required for ribavirin and puromycin, respectively. Interferons were not able to totally inhibit the viral activity in the concentration range tested (up to 10 mg/ml). However, the drug combination identified by the Gur Game reduced the required dosage by 10-fold for individual drug. For example, only 12  $\mu$ g/ml of ribavirin (Fig. 5a) is needed in combinatory drugs, but 100  $\mu$ g/ml of ribavirin (Fig. 5b) is needed for single-drug treatment for 100% inhibition of viral infection. Fig. 5c shows the percentage of viral inhibition for applying single drugs at the concentrations in the potent combination. The data indicate the effectiveness of using drug combinations for inhibiting the viral activity. Inhibiting viral activity with low-dosage combinations provides new opportunities in antiviral therapeutics, because high dosage always associates with cytotoxicity and other side effects on biological systems. As shown



cells (data not shown). For the case of BAFF, it had a minimal effect on NF- $\kappa$ B activity with or without the potent cytokine combination. It was also very interesting to note that the Gur Game suggested lower and lower concentrations of both EGF and BAFF as the iterations proceeded (Fig. 4a). Therefore, the Gur Game algorithm confidently locates the most favorable concentrations for each cytokine, and there is no indication that a more effective combination exists in the entire search space. These data also indicate that the effects of individual cytokines are not additive in the combinatorial tests and the interactions among pathways are nonlinear.

With a stochastic search algorithm to use the output information obtained from the biological response, the closed-loop optimization approach can effectively search for a potent drug mixture without the need for detailed information about the effects of each agent on the networks of pathways. We also found that a much lower dosage is required with the drug mixture compared with individual drugs in the viral infection experiment. In addition, new phenomena can be identified for furthering our understanding of the complex nonlinear interactions in a broad class of biological systems with this approach.

## Methods

**Materials.** Cell culture medium was supplied by Cellgro. Plasmid was purchased from Clontech. Lipofectamine 2000 transfection reagent was purchased from Invitrogen. All other reagents and chemicals were supplied by Sigma unless stated otherwise.

**Viral Infection.** GFP-tagged vesicular stomatitis virus (VSV) was prepared by propagation of virus on confluent monolayers of MDCK cells. Supernatant from infected cells were cleared of debris by centrifugation and spun at  $>100,000 \times g$  through a 25% sucrose cushion by using a Beckman SW28 rotor for 2 h. Virus pellet was gently rinsed and resuspended in PBS. Viral titers were determined by using standard plaque assay procedures on monolayers of MDCK cells. For all experimental infections cells were incubated with viral inoculums at a multiplicity of infection of 1.

**Plasmid Construction and Cell Line Establishment.** The expression construct pCEP4-NF- $\kappa$ B-d2EGFP was generated by cutting out the NF- $\kappa$ B-d2EGFP fragment from pNF- $\kappa$ B-d2EGFP vector at BglII and AclI sites and inserting it into pCEP4 vector, which has EBNA-1 and oriP to maintain episomal DNA replica-

tion (Invitrogen). pNF- $\kappa$ B-d2EGFP vector has a kappa enhancer element ( $\kappa$ B<sub>4</sub>) located in the promoter region of a d2EGFP reporter gene (a destabilized variant of the enhanced green fluorescent protein with a half-life of 2 h) (30). pCEP4 vector expresses a Hygromycin B drug selection marker. The resulting construct pCEP4-NF- $\kappa$ B-d2EGFP was transfected into human embryonic kidney 293T cells by using Lipofectamine 2000 (Invitrogen) and normal cell culture media supplemented with 200  $\mu$ g/ml Hygromycin B (Invitrogen) was used to establish the cell line 293T/NF- $\kappa$ B-d2EGFP.

**Cell Culture.** 293T/NF- $\kappa$ B-d2EGFP cells were grown in DMEM with 10% FBS (Omega), 500 IU/ml Penicillin (Cellgro), 500  $\mu$ g/ml Streptomycin (Cellgro) supplemented with 200  $\mu$ g/ml Hygromycin B in 5% CO<sub>2</sub> at 37°C. The cells have a doubling time of  $\approx$ 1 day and we split them every 3–4 days to avoid confluence. For 96-well-plate experiments, cells were cultured in the plate overnight and allowed to reach  $\approx$ 80% confluence. The cells were stimulated with the appropriate concentration of cytokines for 1 h and washed with fresh media. Fluorescence measurements were performed 7 h after stimulations, when the fluorescence intensity reaches maximum value.

**Microfluidics.** A microfluidic platform has been developed to implement the closed-loop optimization approach. Microfluidic channels were fabricated by micromolding of polydimethylsiloxane (PDMS) (Sylgard, 184) on photoresist master. The masters for micromolding were fabricated by photolithography of positive photoresist SJR 5740 (MicroChem, 41001). Three layers of photoresist were spun on the glass substrate to achieve a final thickness of 60  $\mu$ m. After curing, the PDMS replicas were carefully peeled off from the master. The channels were sealed with a 0.17-mm-thick cover glass. The PDMS replicas and the glass pieces were oxidized for 1 min in a plasma cleaner (Harrick, PDC-001). The two layers were immediately brought into contact to achieve irreversible sealing of the channels.

The microfluidic channel is loaded inside a closed chamber (Instec Inc., HCS60-STC20A) with temperature control, adjusted to 37°C during cell culture experiment. The chamber is supplied with 5% CO<sub>2</sub> mixed with air. The diffusivities for O<sub>2</sub> and CO<sub>2</sub> in PDMS are  $4.1 \times 10^{-5}$  and  $2.6 \times 10^{-5}$  cm<sup>2</sup>/sec, respectively. More information is available in the *SI Appendix*.

**ACKNOWLEDGMENTS.** We thank Dr. Steve Ho for his invaluable suggestions in the implementation of the control algorithm. This work was supported in part by the National Institutes of Health (NIH) through the NIH Roadmap for Nanomedicine (PN2 EY018228) and, in part, by the Institute for Cell Mimetic Space Exploration (CMISE; NCC 2-1364), a National Aeronautics and Space Administration (NASA) University Research, Engineering and Technology Institute (URETI) program.

- De Francesco R, Migliaccio G (2005) Challenges and successes in developing new therapies for hepatitis C. *Nature* 436:953–960.
- Sawyer CL (2007) Mixing cocktails. *Nature* 449:993–996.
- Izumi Y, Xu L, di Tomaso E, Fukumura D, Jain RK (2002) Tumor biology—Herceptin acts as an anti-angiogenic cocktail. *Nature* 416:279–280.
- Blakey GE, et al. (2004) Pharmacokinetic and pharmacodynamic assessment of a five-probe metabolic cocktail for CYPs 1A2, 3A4, 2C9, 2D6 and 2E1. *Br J Clin Pharmacol* 57:162–169.
- Chesney MA, Ickovics J, Hecht FM, Sikipa G, Rabkin J (1999) Adherence: A necessity for successful HIV combination therapy. *AIDS* 13:S271–S278.
- Dancey JE, Chen HX (2006) Strategies for optimizing combinations of molecularly targeted anticancer agents. *Nat Rev Drug Discovery* 5:649–659.
- Decker S, Sausville EA (2005) Preclinical modeling of combination treatments: Fantasy or requirement? *Ann N Y Acad Sci* 1059:61–69.
- Nakanishi C, Toi M (2005) Nuclear factor-kappa B inhibitors as sensitizers to anticancer drugs. *Nat Rev Cancer* 5:297–309.
- Stancovski I, Baltimore D (1997) NF-kappa B activation: The I kappa B kinase revealed? *Cell* 91:299–302.
- Queipo NV, et al. (2005) Surrogate-based analysis and optimization. *Prog Aerospace Sci* 41:1–28.
- Pannetier J, Bassasalsina J, Rodriguezcarvajal J, Caignaert V (1990) Prediction of crystal-structures from crystal-chemistry rules by simulated annealing. *Nature* 346:343–345.
- Forrest S (1993) Genetic algorithms—Principles of natural-selection applied to computation. *Science* 261:872–878.
- Bonabeau E, Dorigo M, Theraulaz G (2000) Inspiration for optimization from social insect behaviour. *Nature* 406:39–42.
- Tsetlin ML (1963) Finite automata and the modeling of the simplest forms of behavior. *Uspekhi Matem Nauk* 8:1–26.
- Hartmann AK, Rieger H (2002) in *Optimization Algorithms in Physics* (Wiley, Berlin).
- Tung B (1994) Distributed control using simple automata. PhD dissertation (University of California, Los Angeles).
- Tung B, Kleinrock L (1996) Using finite state automata to produce self-optimization and self-control. *IEEE Trans Parallel Distrib Syst* 7:439–448.
- Slepchenko BM, Schaff JC, Carson JH, Loew LM (2002) Computational cell biology: Spatiotemporal simulation of cellular events. *Annu Rev Biophys Biomol Struct* 31:423–441.
- Gillespie B, Plaxco KW (2004) Using protein folding rates to test protein folding theories. *Annu Rev Biochem* 73:837–859.
- Fernandez M, Porosnicu M, Markovic D, Barber GN (2002) Genetically engineered vesicular stomatitis virus in gene therapy: Application for treatment of malignant disease. *J Virol* 76:895–904.
- Malinin NL, Boldin MP, Kovalenko AV, Wallach D (1997) MAP3K-related kinase involved in NF-kappa B induction by TNF, CD95 and IL-1. *Nature* 385:540–544.
- Siebenlist U, Franzoso G, Brown K (1994) Structure, regulation and function of NF-kappa-B. *Ann Rev Cell Biol* 10:405–455.
- Kan H, Xie ZR, Finkel MS (1999) TNF-alpha enhances cardiac myocyte NO production through MAP kinase-mediated NF-kappa B activation. *Am J Physiol* 277:H1641–H1646.
- Marcus JS, Karackattu SL, Fleegal MA, Summers C (2003) Cytokine-stimulated inducible nitric oxide synthase expression in astroglia: Role of Erk mitogen-activated protein kinase and NF-kappa B. *Glia* 41:152–160.
- Biswas DK, Cruz AP, Gansberger E, Pardee AB (2000) Epidermal growth factor-induced nuclear factor kappa B activation: A major pathway of cell-cycle progression in estrogen-receptor negative breast cancer cells. *Proc Natl Acad Sci USA* 97:8542–8547.
- Izumi H, et al. (1994) Cross-talk of tumor-necrosis-factor-alpha and epidermal growth-factor in human microvascular endothelial-cells. *Exp Cell Res* 214:654–662.
- Banan A, et al. (2003) Evidence that nuclear factor-kappa B activation is critical in oxidant-induced disruption of the microtubule cytoskeleton and barrier integrity and that its inactivation is essential in epidermal growth factor-mediated protection of the monolayers of intestinal epithelia. *J Pharmacol Exp Ther* 306:13–28.
- Claudio E, Brown K, Park S, Wang HS, Siebenlist U (2002) BAFF-induced NEMO-independent processing of NF-kappa B2 in maturing B cells. *Nat Immunol* 3:958–965.
- Hoffmann A, Levchenko A, Scott ML, Baltimore D (2002) The I kappa B-NF-kappa B signaling module: Temporal control and selective gene activation. *Science* 298:1241–1245.
- Li XQ, et al. (1998) Generation of destabilized green fluorescent protein transcription reporter. *J Biol Chem* 273:34970–34975.

## Principle of the Gur Game

The principle of the Gur Game (1) is based on biased random walks of finite-state automata (a set of drugs). The automata describe a set of drugs with assigned concentration values and a set of rules is included for determining how the concentration of the drug switches from one value to the other. Each drug concentration is referred as a state of the automaton. The overall goal of the automata design is to have the drugs to self-organize (choose the optimal concentrations) in an attempt to maximize the overall system performances (desired biological responses indicated by biomarkers). The biological response is transformed into a reward function, which describes the probability of the drug to switch between different concentrations.

To understand the principle of the Gur Game algorithm, it is helpful to consider an example for choosing the concentration of a drug to maximize the antiviral activity (AVA). We design a finite-state automaton with only two states, i.e., one drug with two concentrations (SI Fig. 7). Assuming the two concentrations,  $C_1$  and  $C_2$ , of the drug will give antiviral activities of  $AVA_1$  and  $AVA_2$ , respectively. A reward function can be defined to map  $AVA_1$  and  $AVA_2$  to probabilities of  $r_1$  and  $r_2$  of the drug to be rewarded. For example, the percentage of cells not being infected (the AVA) can be considered to be the probability of the drug being rewarded (i.e., the reward function). At each iteration, the drug can either be awarded or penalized. If the concentration  $C_1$  is applied, then the drug will have a chance of  $r_1$  to be rewarded. The drug then has a probability of  $(1 - r_1)$  and  $(1 - r_2)$  to receive a penalty in the corresponding states. If the drug is rewarded, it chooses to keep the same concentration. Otherwise, the drug concentration will be switched from one concentration to the other. Because a concentration that gives higher AVA will have higher chance to be rewarded, the drug concentration will have a higher chance to stay in a concentration with high AVA. If the drug concentration gives a low AVA, the drug will have a high chance to be switched to the other concentration. In general, this design encourages the drug to choose a concentration with high AVA because the drug has a higher chance of being rewarded.

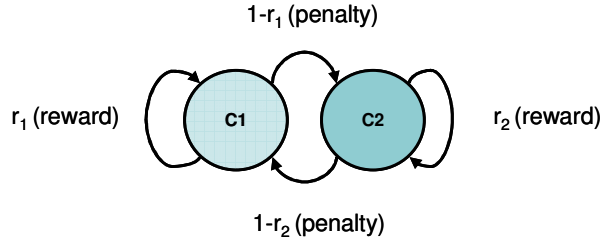


**Fig. 7.** A simple automaton design with two states (one drug with two possible concentrations). The drug concentration stays the same if the automaton (drug) is rewarded. Otherwise (penalized), the drug is switched to the other concentration.

The asymptotic behavior of the drug can be modeled by using the Markov chain analysis (2). We define  $\pi_1$  and  $\pi_2$  to be the steady-state probabilities of being in drug concentrations of C1 and C2, respectively. The fact that the probabilities sum to unity gives Eq. 1 (the drug chooses either C1 or C2). Equating the transition probabilities (switching from one concentration to the other) leads to Eq. 2. Solving the equations gives the steady-state probability of choosing C2 in Eq. 3.

$$\pi_1 + \pi_2 = 1 \quad [1]$$

$$\pi_1(1-r_1) = \pi_2(1-r_2) \quad [2]$$

$$\pi_2 = \frac{1-r_1}{2-r_2-r_1} \quad [3]$$

If we assume drug concentrations, C1 and C2, give AVA of 0.4 and 0.8 and the AVA is directly defined as the reward probability (i.e.,  $r_1 = 0.4$  and  $r_2 = 0.8$ ), the steady state probability of the drug to choose the concentration C2 will be 0.75, whereas the probability of choosing the concentration C1 is 0.25. Therefore, the drug chooses C2 (high AVA) three times more often than C1 (low AVA). In other words, the drug self-organizes to spend more time in a concentration with a higher AVA level.

The same idea can be extended to the general case of a drug with multiple concentrations. In general, the drug moves to the system state toward the center of the state space if penalized, and away from the center if rewarded (see SI Fig. 8). This design allows the drug to “detect” promising trends of drug concentrations. SI Fig. 8 shows a drug with  $2n$  states (from  $-n$  to  $+n$ ) and each state is assigned with a different concentration. If the drug is rewarded, the automaton moves from state  $i$  to  $i + 1$  if  $i$  is positive or from  $i$  to  $i - 1$  if  $i$  is negative. The automaton stays in state  $n$  or  $-n$  if it is in either one of those states. For a penalty, it moves from state  $1$  to  $-1$  or *vice versa* if it is at one of the state, otherwise it moves from state  $i$  to  $i - 1$  if  $i$  is positive, or from  $i$  to  $i + 1$  if  $i$  is negative. If a low drug concentration has a high AVA (being reward), the automaton attempts to further improve the performance by searching for even lower concentrations. If the drug concentration goes too low and the drug has a high chance to be penalized, the drug concentration will be driven back to a relatively higher concentration. In the case of multiple drugs, the drugs collectively search for a mixture with high AVA (being reward). This framework provides a very rapid and robust control approach for optimizing drug combinations. For complete details, the reader is referred to original discussions of the Gur Game (1-4).

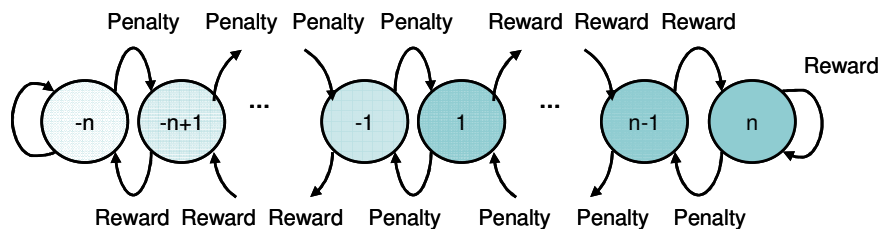


**Fig. 8.** An automaton design with multiple concentrations.

## Implementation of the Gur Game

**Flowchart Representation of the Gur Game.** SI Fig. 9 shows a flowchart representation of the Gur Game applied in this study. The study started with initiation of the concentrations of a mixture. Then, an experiment using the drug mixture was performed to estimate the reward value (the probability of the drug being rewarded or penalized). In the VSV experiment, the reward value was estimated according to the percentage of cells not expressing GFP (i.e., not infected by

the virus). In the NF- $\kappa$ B experiment, the peak GFP intensities were normalized to map the system state from 0 to 1 with high GFP intensities corresponding to values nearer 1. The GFP value was the average fluorescence intensity of individual cells measured by a 16 bit cooled CCD camera (Photometric CH350L). Intensity values of individual cells were measured by using ImageJ. The GFP data are the average response of  $\approx 100$  cells. The data are normalized to be the reward value. The normalization value was determined experimentally and iteratively such that the reward value is between 0 and 1. A random number from 0 to 1 was generated and was compared with the reward value for each automaton. A set of predefined rules of the automata design were used to determine the drug concentrations in the subsequent iteration to probabilistically drive the drugs toward viral inhibition or high NF- $\kappa$ B activity. The concentrations of the drugs were then determined for the next iteration. The process is repeated for each drug during each iteration. The process can be terminated when the system states are spending a large portion of time in some states and/or when a preset performance of the system is reached. Otherwise, a new iteration is initiated and the process repeats.

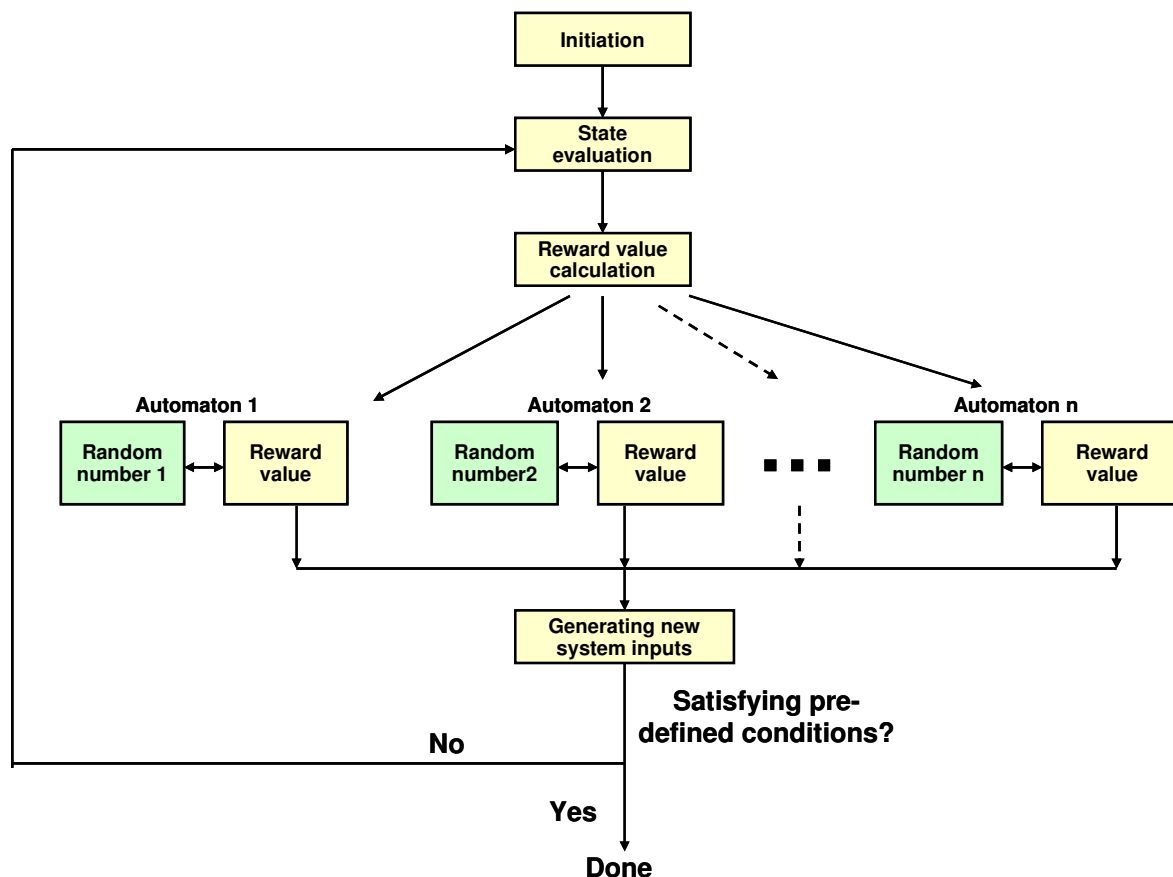


**Fig. 9.** Flowchart representation of the Gur Game algorithm.

**Drug Concentrations for the Antiviral Experiment.** We have designed four sets of experiments for searching the antiviral drug combinations. The automata design is shown in SI Tables 2 to 4. Set 1 and set 2 have 6 states (concentrations) for each automaton (drug). Set 3 and set 4 have the same search space, which has 10 states for each automaton. Each state represents a drug concentration shown in the SI Tables 2 to 4 and the corresponding automata are shown below. We have also applied different initial conditions in the experiments (SI Table 5). For set 1 and set 2, initial concentrations were zero for all agents and random initializations were applied for set 3 and set 4.

**Tables 2-4.** Automata design for antiviral drug cocktails.

**Table 2. Search space for set 1**

State	-3	-2	-1	1	2	3
IFN $\alpha$ , pg/ml	0	1.3	6.5	13	65	130
IFN $\beta$ , ng/ml	0	0.1	0.5	1	5	10
IFN $\gamma$ , ng/ml	0	10	50	100	500	1000

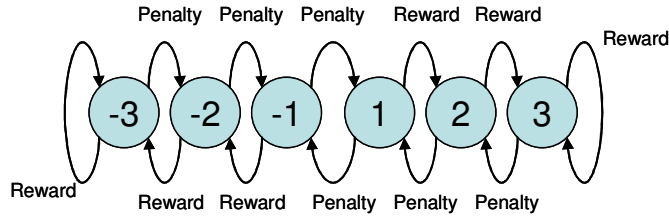


**Table 3. Search space for set 2**

State	-3	-2	-1	1	2	3
IFN $\alpha$ , pg/ml	0	0.65	1.3	6.5	13	65
IFN $\beta$ , ng/ml	0	0.05	0.1	0.5	1	5
IFN $\gamma$ , ng/ml	0	5	10	50	100	500
Puromycin, $\mu$ g/ml	0	0.125	0.25	1.25	2.5	12.5

Ribavirin, $\mu\text{g/ml}$	0	0.5	1	5	10	50
-----------------------------	---	-----	---	---	----	----

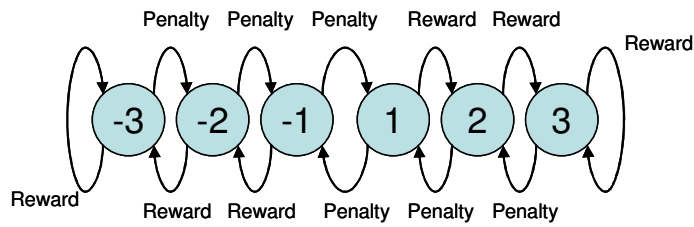


**Table 4. Search space for set 3 and set 4**

State	-5	-4	-3	-2	-1	1	2	3	4	5
IFN $\alpha$ , pg/ml	0	0.65	1.3	3.9	7.8	15.6	32.5	65	130	260
IFN $\beta$ , ng/ml	0	0.05	0.1	0.3	0.6	1.2	2.5	5	10	20
IFN $\gamma$ , ng/ml	0	5	10	30	60	120	250	500	1000	2000
Puromycin, $\mu\text{g/ml}$	0	0.125	0.25	0.75	1.5	3	6.25	12.5	25	50
Ribavirin, $\mu\text{g/ml}$	0	0.5	1	3	6	12	25	50	100	200

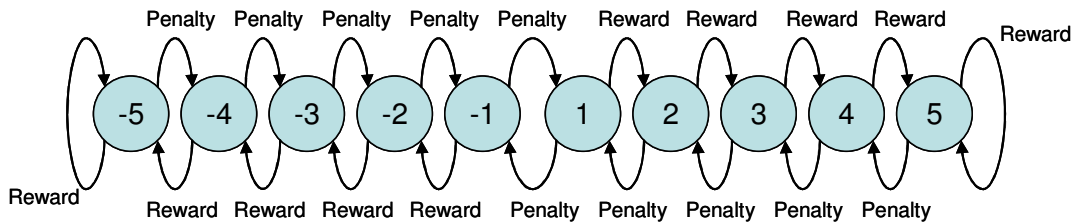


**Table 5. Initial conditions of the experiment.**

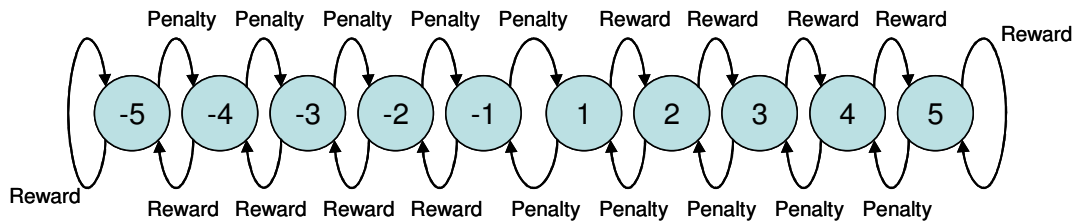
	Set 1	Set 2	Set 3	Set 4
IFN $\alpha$ , pg/ml	0	0	7.8	1.3
IFN $\beta$ , ng/ml	0	0	0.6	1.2
IFN $\gamma$ , ng/ml	0	0	60	1000
Puromycin, $\mu\text{g/ml}$	-	0	1.5	0.75
Ribavirin, $\mu\text{g/ml}$	-	0	6	12

**Cytokine Concentrations for Regulating NF- $\kappa$ B Activity.** In this Gur Game implementation, we assigned a different drug concentration to each state of the automaton. This allows for a search technique that rapidly moves around the search space and is less likely to be trapped in any one state. All cytokines were represented by automata with 10 discrete states (0, 0.25, 0.5, 1,

2.5, 5, 10, 25, 50, and 100) ng/ml, which span across three orders of magnitude, in the NF- $\kappa$ B experiment (SI Table 6). The states of automata were designed for maximizing the range of cytokine concentrations being tested while maintaining the resolution for searching the optimal cytokine concentration. During each iteration, a random number was generated for each automaton. The numbers were compared with the reward value. If the reward value was greater than the random number, the automaton was rewarded. Otherwise, the automaton was penalized. The automaton then decided the state in the next iteration according to the automaton design. In general, the state moves toward the center if penalized and away from the center if rewarded.

**Table 6. Automata design for manipulating NF- $\kappa$ B activity**

State	-5	-4	-3	-2	-1	1	2	3	4	5
TNF $\alpha$ , ng/ml	0	0.25	0.5	1	2.5	5	10	25	50	100
TNF $\beta$ , ng/ml	0	0.25	0.5	1	2.5	5	10	25	50	100
IL-1 $\alpha$ , ng/ml	0	0.25	0.5	1	2.5	5	10	25	50	100
IL-1 $\beta$ , ng/ml	0	0.25	0.5	1	2.5	5	10	25	50	100
EGF, ng/ml	0	0.25	0.5	1	2.5	5	10	25	50	100
BAFF, ng/ml	0	0.25	0.5	1	2.5	5	10	25	50	100



### Characteristics of the Gur Game Algorithm

In most biological systems, a complete model of the governing network is often not available and only partial information of the system of interest is known. The Gur Game provides a generic mechanism for regulating these complex systems without the requirement of a preassumed model of the system or knowledge of how the system performance depends on the variables being manipulated. Unlike gradient search methods, the Gur Game drives the system state to higher performance probabilistically, instead of deterministically. The probabilistic characteristic

of the Gur Game allows the system state to “escape” from local optima and search for the global optimum in the search space. For the same reason, the algorithm performs robustly in a noisy environment. This robustness is critical for controlling biological systems, which are intrinsically noisy (5).

Another important characteristic of the Gur Game is that the optimality is determined by the average behavior (1, 2). The automata states spend more time at states with high reward probability, i.e., good system performance. There is no dynamic difference between the transient behavior of the system and its steady-state behavior. This feature enables the system to respond to a changing population and/or reward function. It is interesting to compare this characteristic with the robustness in cellular functions (6). In general, the automata and the reward function (mapping between the system performance and reward probability) should be adjusted to fine tune the balance between the robustness, converging rate, and the ability to escape from local traps (1, 2). For distributed control and other self-organizing systems, it is preferable to have small step size such that the system locks into desired behaviors (4). The trade-off is that more steps are required for the system to reach an optimal solution. For searching and optimization experiments, increasing the “randomness” with larger step size improves the chance that the automata will escape from local optima and rapidly search for the global solution (7).

### **Reward Function and Automata Design**

**Reward Function.** A key concept in the Gur Game is the reward function, which is a global figure of merit. Basically, the reward function is a measurement of the system performance as a whole. Similar concepts can be found in other optimization approaches. For instance, it is called a fitness function in genetic algorithms (8) and an energy function in simulated annealing (9). It is one of the most important parts for the success of a closed-loop optimization experiment. The design of a reward function critically determines how well the algorithm is able to solve the problem. In the VSV experiment, the reward function is the percentage of cells not being infected (indicated by GFP expression). In the NF- $\kappa$ B experiment, the reward function is estimated by the NF- $\kappa$ B activity (indicated by the fluorescence intensity). A deep appreciation of the reward function not only provides the scientist extra freedom to improve the search but also

broadens the applicability to a wide class of biological systems. To design a reward function, a set of systemic output indicators should be defined. In most cases, phenotypic responses such as proliferation rates, gene expressions, and differentiation efficiency can be directly considered as the reward function. It should also be noted that the reward function can be nonlinearly mapped to the system performance to improve the search efficiency and the converging rate. In general, the reward function of the system can be multimodal, nonlinear, and even discontinuous.

**Automata Design.** As discussed, the design of the automata is an important component in the realization of the optimization process. Concentration of drugs (states of the automata) can be assigned depending on the range of the drug concentrations intended to be explored. The values can be linear, logarithmic, or other nonlinear functions depending on the nature of the problem. The number of states should be designed according to the requirements of the converging rate, randomness, and resolution. Unlike, surrogate-based optimization, experimental implementation of a closed-loop optimization scheme does not require “training” of inputs. Extension of the input ranges (drug selection and concentration) can be performed by including extra automata and states of the automata. Another advantage of the stochastic search algorithm is that the converging rate is usually maintained during extension of the input ranges.

**Systems with Multiple Outputs.** For optimizing multiple parameters, the vector norm or a weighted average of these parameters can be applied to optimize the overall performance. Other schemes can also be applied to account for multiple output parameters. In general, the more information, such as some key molecular components, that is known about the system, the easier to design the experiment. Unfortunately, these parameters are usually not clear and the reward functions in some problems may not be straightforward. Most cases require a slight modification of the problem to define the reward function. If necessary, multiple generations of the closed-loop optimization experiment can be performed systemically to identify the appropriate reward functions. In the current study, we have demonstrated the optimization of two different biological systems. Other examples of the implementation of the Gur Game can be found elsewhere (1, 2).

## **Microfluidic Channel and Cell Culture**

**Microfluidic Cell Culture System.** The microfluidic channel is integrated into a cell culture chamber (Instec Inc, HCS60-STC20A) with temperature control at 37°C. The chamber is mounted on a fluorescence microscope (Nikon TE200) for real-time monitoring. Fluorescence images were captured with a 1024 × 1024 pixel, 16-bit cooled CCD camera (Photometric CH350L). Mini peristaltic pumps (Instech Inc, P625-10638), pressure transducer (Honeywell, ACSX05DN), and temperature probe (Omega, DP460) were connected to the chamber and were centrally controlled by a Labview software (National instruments). The entire setup was sitting inside a vertical clean bench, which prevents contamination from the environment (SI Fig. 10).

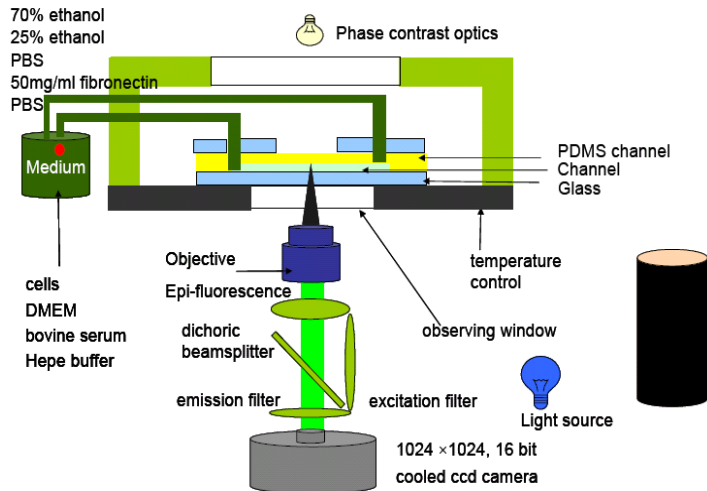


**Fig. 10.** Microfluidic channel and cell culture system.

**Preparation Microchannel for Cell Culture.** Before the experiment, the channels were sterilized by flowing 70% ethanol for 30 min. The channels were then washed with 25% ethanol, DI water, and PBS each for 10 min. The channel surface was then incubated with 200 mg/ml fibronectin for >1 h to modify the channel surface for promoting cell adhesion. Culture media (DMEM without phenol red) was flowed into the channel and the channel was then filled with a suspension of 293T cells. The cells were allowed to adhere to the channel surface for 4-6 h and medium was then perfused at a flow rate of 0.9 ml/min. At this flow rate, the cells experienced wall shear stress of 0.02-0.5 dyne/cm<sup>2</sup> as estimated by numerical simulation (CFDRC CFD-ACE+). This value was below the typical range of shear stress for affecting normal cell functions

or inducing other cellular responses. The cells were allowed to culture in the device overnight before the experiment. The cells could be cultured for an extended period and reached a high confluency. With normal culture conditions, the cells had similar morphologies and growth rates compared to those in cell culture dish.

1. Tsetlin ML (1963) Finite automata and the modeling of the simplest forms of behavior. *Uspekhi Matem Nauk* 8:1-26.
2. Tung B, Kleinrock L (1996) Using finite state automata to produce self-optimization and self-control. *IEEE Trans Parallel Distrib Syst* 7:439-448.
3. Tsetlin ML (1963).Finite automata and modeling the simplest forms of behavior. *Uspekhi Matem Nauk* 8:1-26.
4. Tung B (1994) Distributed control using simple automata. University of California, Los Angeles.
5. Rao CV, Wolf DM, Arkin AP (2002) Control, exploitation and tolerance of intracellular noise. *Nature* 420:231-237.
6. Stelling J, Sauer U, Szallasi Z, Doyle FJ, Doyle J (2004) Robustness of cellular functions. *Cell* 118:675-685.
7. Ho S, Nassef H, Pornsinsirak N, Tai YC, Ho CM (2003) Unsteady aerodynamics and flow control for flapping wing flyers. *Prog Aerospace Sci* 39:635-681.
8. Forrest S (1993) Genetic algorithms—Principles of natural-selection applied to computation. *Science* 261:872-878.
9. Kirkpatrick S, Gelatt CD, Vecchi MP (1983) Optimization by simulated annealing. *Science* 220:671-680.

